NASA
Technical Memorandum 78057

# Transformation of Surface Albedo to Surface - Atmosphere Albedo and Irradiance, and their Spectral and Temporal Averages

Myron L. Nack and Robert J. Curran

(NASA-TM-78057) TRANSFORMATION OF SURFACE ALBEDO TO SURFACE: ATMOSPHERE SURFACE AND IRRADIANCE, AND THEIR SPECTRAI AND TEMPORAL AVERAGES (NASA) 49 p HC A03/MF A01 CSCL 04A

N79-16476

Unclas
G3/46 13571

AUGUST 1978

National Aeronautics and
Space Administration

Goddard Space Flight Center
Greenbelt, Maryland 20771

# TRANSFORMATION OF SURFACE ALBEDO TO SURFACE – ATMOSPHERE ALBEDO AND IRRADIANCE, AND THEIR SPECTRAL AND TEMPORAL AVERAGES

Myron L. Nack

Robert J. Curran

## ABSTRACT

The dependence of the albedo at the top of a realistic atmosphere upon the surface albedo, solar zenith angle, and cloud optical thickness is examined for the cases of clear sky, total cloud cover, and fractional cloud cover. The radiative transfer calculations of Dave and Braslau (1975) for particular values of surface albedo and solar zenith angle, and a single value of cloud optical thickness are used as the basis of our parametric albedo model. The question of spectral and temporal averages of albedos and reflected irradiances is addressed, and unique weighting functions for the spectral and temporal albedo averages are developed.

CONTENTS



ILLUSTRATIONS

ILLUSTRATIONS (Continued)



TABLES

# TRANSFORMATION OF SURFACE ALBEDO TO SURFACE — ATMOSPHERE ALBEDO AND IRRADIANCE, AND THEIR SPECTRAL AND TEMPORAL AVERAGES

## 1. INTRODUCTION

Radiation transfer calculations form the coupling between satellite determined radiation budget components and the physical processes incorporated in climate models. The use of exact radiation transfer calculations in such climate models is often frustrated by the volume of tabular and graphical data produced in the transfer calculation, and the non-analytic nature of the solution. The present study is the result of an effort to match the needs of climate modelers to the available radiation budget data by means of a parameterization of exact radiation transfer calculations. A recent set of calculations of this type was performed by Dave and Braslau (1974, 1975), hereafter referred to as DB, for a realistic atmosphere with and without a stratus cloud layer. Both sets of calculations are here parameterized to relate surface-atmosphere albedo to surface albedo in terms of linear equations.

A linear albedo relationship for the cloud free atmosphere has been developed by Vinnikov (1965) and used quite extensively by Budyko (see Budyko (1974)). The linear relationships of Vinnikov are traceable back to 1962; a time when measurements of the optical properties of the atmosphere were somewhat incomplete. However, that formulation has been found to agree almost exactly with the present parameterization for a solar zenith angle 60°. In a sense, the present formulation extends the work of Vinnikov to a more general dependence on surface albedo, solar zenith angle and cloud optical thickness. In sections 2 and 3 of this paper "cloudy" means total cloud cover and surface albedo is assumed to be horizontally homogenous. In section 4 we extend our analysis to include fractional cloud cover and fractional surface albedo cover.

In subsequent work, Curran, Wexler and Nack (1978), hereafter referred to as CWN (1978), apply the derived albedo transformations to a monthly zonal surface albedo model. This application produces a monthly zonal cloud free and cloudy surface-atmosphere system albedo which is used in the determination of monthly zonal cloud fractions. The modeled albedos are combined with the measured data supplied by the Nimbus-6 Earth Radiation Budget (ERB) experiment (see Smith et al., 1977) to form the cloud fractions. These cloud fractions are necessarily determined for a fixed local time due to the sun-synchronous orbit of Nimbus-6.

The final effort in this series is the determination of the daily and monthly averaged, reflected zonal shortwave irradiances. The irradiances are formed by assuming the cloud fractions to be constant over all local times throughout the month. Daily integrations of the irradiances are made using the averaging techniques developed in this present report. These techniques make use of our solar zenith angle parameterization. They could include time dependent cloud fraction data, but will use our ERB albedo determined cloud fractions due to a lack of time dependent data.

## 2. ALBEDO TRANSFORMATIONS FOR CLEAR AND CLOUDY ATMOSPHERES

The albedo of the earth-atmosphere system is defined as the ratio of reflected solar irradiance to that incident from the sun. For the present study the system albedo, denoted $A_s$ for cloud free and $A_c$ for cloudy, is assumed to be a function of the surface albedo a, the solar zenith angle $\theta_0$ and a cloud optical thickness $\tau_c$. The surface albedo a is defined in a manner similar to the system albedo, i. e. , the surface albedo a is the ratio of the irradiance reflected from a surface to that incident upon it. For the purposes of the present study, the surface is assumed to be a Lambert reflector. It should be noted that the refectance of natural surfaces may depend on the angular distribution of the incident radiation. This latter dependency is assumed to be second order to the parameterization being investigated. The cloud optical thickness is defined at 0. 555 $\mu$m.

To fit the results of Dave and Braslau (1974, 1975) linear functions are chosen as follows:

$$A_s(a, \theta_0) = m_s(\theta_0)a + A_s(0, \theta_0), \tag{1}$$

$$\begin{aligned} A_c(a, \theta_0, \tau_c) &= m_c(\theta_0)g(\tau_c)a + A_c(0, \theta_0, \tau_c) \\ &= A_c[a, \theta_0, A_c(0, 0, \tau_c)]. \end{aligned} \tag{2}$$

Terms dependent on higher powers of a were neglected since the fit resulting from the linear functions seemed satisfactory.

Equation (2) indicates that the explicit $\tau_c$ dependence of A can be replaced by an implicit dependence on $A_c$ (0, 0, $\tau_c$ ). The slope factor of Eq. 1 depends only on solar zenith angle $\theta_0$. However, the slope factor of Eq. 2 has been separated into a factor dependent on solar zenith angle $m_c(\theta_0)$, and a factor dependent on cloud optical thickness $g(\tau_c)$.

Since the Dave and Braslau results were computed at only one optical thickness ($\tau_c = 3.35$), the present formulation sets $g(3.35) = 1.0$. To accomodate other values of $\tau_c$ or $A_c(0, 0, \tau_c)$ we require g to decrease as its argument increases. A function which satisfies this constraint is:

$$g(\tau_c) = g[A_c(0, 0, \tau_c)] = \frac{A_c(0, 0, 3.35)}{A_c(0, 0, \tau_c)} \tag{3}$$

The purpose of the function g is to dampen the dependence of $A_c(a, \theta_0, \tau_c)$ on a as $\tau_c$ increases. A further constraint on g is

$$A_c(a, \theta_0, \tau_c) < 1.0 \tag{4}$$

for all a including the extreme case of a = 1.0, since the realistic atmospheric model of Dave and Braslau (1974, 1975) that we parameterize includes absorption.

The intercepts $A_s(0, \theta_0)$ and $A_c(0, \theta_0, 3.35)$ of Eqs. 1 and 2 are found using Table 4 of Dave and Braslau (1974) for the atmospheric models C1 and C1-ST, respectively. A polynomial fit to these data was made as follows:

$$A_s(0, \theta_0) = 0.0483 + (1.087 \times 10^{-5})\theta_0^2 - (2.219 \times 10^{-9})\theta_0^4 + (6.776 \times 10^{-13})\theta_0^6 \tag{5}$$

and

$$A_c(0, \theta_0, \tau_c) = A_c(0, 0, \tau_c) + (4.906 \times 10^{-5})\theta_0^2 \quad (6)$$

with $A_c\ (0,\ 0,\ \tau_c\ ) = 0.1940$ in this section. The solar zenith angle $\theta_0$ is here measured in degrees. The solar zenith angle independent terms of Eqs. 5 and 6 are identically equal to the Dave and Braslau values for $\theta_0 = 0°$. The remaining coefficients of Eqs. 5 and 6 were obtained by performing a least squares difference minimization fit of the polynomial to the tabular values of Dave and Braslau. The solar zenith angle dependent values of $A_s\ (0,\ \theta_0)$ and $A_c\ (0,\ \theta_0,\ \tau_c)$ using Eqs. 5 and 6 are shown in Table 1. These intercept values are also shown graphically in Fig. 1.

Table 1

The Intercepts and Slopes of Linear Albedo Transformations

| $\theta_0$ | $A_s$ | $A_c$ | $m_s$ | $m_c$ |
|---|---|---|---|---|
| 0 | 0.0483 | 0.1940 | 0.7213 | 0.5079 |
| 5 | 0.0486 | 0.1952 | 0.7213 | 0.5037 |
| 10 | 0.0494 | 0.1989 | 0.7213 | 0.4977 |
| 15 | 0.0506 | 0.2050 | 0.7212 | 0.4900 |
| 20 | 0.0523 | 0.2136 | 0.7209 | 0.4804 |
| 25 | 0.0544 | 0.2247 | 0.7203 | 0.4691 |
| 30 | 0.0568 | 0.2382 | 0.7192 | 0.4560 |
| 35 | 0.0595 | 0.2541 | 0.7171 | 0.4411 |

Table 1 (Continued)

| $\theta_0$ | $A_s$ | $A_c$ | $m_s$ | $m_c$ |
|---|---|---|---|---|
| 40 | 0.0628 | 0.2725 | 0.7137 | 0.4245 |
| 45 | 0.0668 | 0.2933 | 0.7083 | 0.4060 |
| 50 | 0.0722 | 0.3167 | 0.7000 | 0.3858 |
| 55 | 0.0796 | 0.3424 | 0.6877 | 0.3638 |
| 60 | 0.0903 | 0.3706 | 0.6700 | 0.3400 |
| 65 | 0.1057 | 0.4013 | 0.6451 | 0.3144 |
| 70 | 0.1280 | 0.4344 | 0.6108 | 0.2870 |
| 75 | 0.1598 | 0.4700 | 0.5644 | 0.2579 |
| 80 | 0.2046 | 0.5080 | 0.5025 | 0.2270 |
| 85 | 0.2666 | 0.5485 | 0.4212 | 0.1943 |
| 90 | 0.3509 | 0.5914 | 0.3157 | 0.1598 |

The slope functions $m_s$ and $m_c$ of Eqs. 1 and 2 are determined by using the above intercept values and making a best fit to the surface albedo dependent results of Dave and Braslau. The best fit is for the angles $\theta_0 = 0°$ and 80° of Table 7 of Dave and Braslau (1974), and $\theta_0 = 60°$ in Fig. 7 of Dave and Braslau (1975). The values obtained by this fitting procedure are shown in Table 1 for these three angles.

The functional relationships which were used to fit the $\theta_0$ dependence of the slope functions for these three angles are given by:

$$m_s(\theta_0) = 0.7213 - (2.180 \times 10^{-9})\theta_0^4 - (4.941 \times 10^{-13})\theta_0^6 , \quad (7)$$

$$m_c(\theta_0) = 0.5079 - (6.596 \times 10^{-4})\theta_0 - (3.565 \times 10^{-5})\theta_0^2 . \quad (8)$$

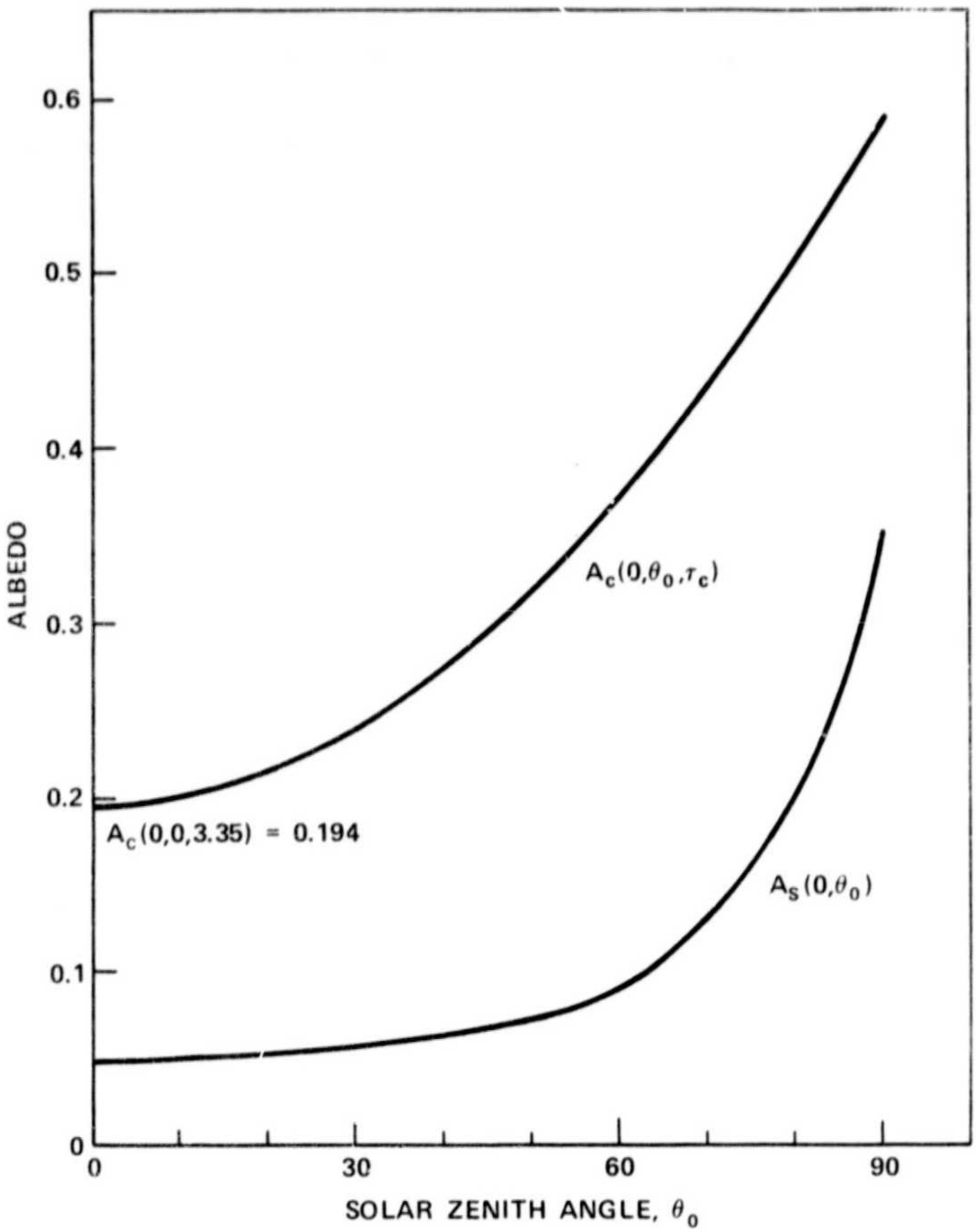


Figure 1. Solar Zenith Angle Dependence of Our Intercept Albedos

The three coefficients of $m_s(\theta_0)$ and $m_c(\theta_0)$ are determined by fitting their values at 0°, 60°, and 80° exactly. Graphs of the slope functions of Eqs. 7 and 8 are shown in Fig. 2, and their values are shown in Table 1.

The $\theta_0$ dependence of both the slopes and intercepts of Eqs. 1 and 2 may now be substituted into those expressions to form the top of the atmosphere albedo for both the cloudy and cloud-free atmosphere. The values of $A_s(a, \theta_0)$, the cloud-free albedo, are given in Table 2 as a function of both arguments. These values are also given in graphical form in Fig. 3. Similar values for the albedo at the top of the cloud obscured atmosphere are shown in Table 3 and displayed graphically in Figure 4.

If we compare the values of $A_s(a, \theta_o)$ in Table 2 with the values of $A_c(a, \theta_o, \tau_c)$ of Table 3 we see that in general $A_c(a, \theta_o, \tau_c) > A_s(a, \theta_o)$. This agrees with our initial intuitive response that the insertion of the cloud layer should increase the albedo at the top of the atmosphere over the corresponding clear sky case. However, a detailed comparison shows that the values above the discriminator line in Table 3 satisfies this inequality, whereas, for values below the discriminator line this inequality becomes reversed and $A_s(a, \theta_o) > A_c(a, \theta_o, \tau_c)$. This is caused by the absorption in the atmospheric model. The optical thickness of the cloud is small enough to allow an amount of radiation through the cloud (for smaller solar zenith angles) to be repeatedly reflected back and forth between the highly reflective surface and the cloud bottom. These multiple reflections in the absorbing atmosphere decrease the amount of radiation that can escape out of the top of atmosphere relative to the clear sky case. When $\theta_o$ is large enough, for each of these values of large surface reflectivity, eventually $A_c > A_s$. This is because the effective optical thickness of the cloud gets large enough to make negligible the proportion of radiation penetrating the cloud and feeling the effect of these multiple reflections with absorption.

The separation of values of $(a, \theta_o)$ in Tables 2 and 3 into sets where $A_c > A_s$ and $A_s > A_c$ leaves a line of values (as shown in Table 3) which satisfy $A_s(a, \theta_o) = A_c(a, \theta_o, \tau_c)$. For these values the ability to distinguish a snow covered surface with or without our cloud layer over it disappears if only albedo measurements are used.

It is noted in Figures 3 and 4 that the top of the atmosphere albedo is always less than unity, in agreement with the fact that the radiation transfer calculations upon which these parameterizations were made, contain contributions due to molecular absorption. The increase in the intercepts with increasing solar zenith angle, or $\partial A_s(0, \theta_0)/\partial\theta_0 > 0$ and $\partial A_c(0, \theta_0, \tau_c)/\partial\theta_0 > 0$, is shown in Figs. 1, 3, and 4, and explained by the increase in scattered radiance due to the greater effective optical depth of an atmosphere in which scattering dominates absorption. As $\theta_0$ increases less radiation reaches the surface. This additional radiation is not lost as a result of the zero surface albedo, and consequently, is available to the atmosphere for either absorption or scattering. For the same reason the slopes decrease as the solar zenith angle increases as is shown in Fig. 2, or $\partial m_s(\theta_0)/\partial\theta_0 < 0$ and $\partial m_c(\theta_0)/\partial\theta_0 < 0$. This is consistent with the sensitivites of the albedos at the top of the atmosphere to the surface albedo, or

$$\partial A_s(a,\theta_0)/\partial a = m_s(\theta_0)$$

$$\partial A_c(a,\theta_0,\tau_c)/\partial a = m_c(\theta_0)g(\tau_c),$$

decreasing as less radiation reaches the surface (due to increasing solar zenith angle).

In general for a fixed surface albedo the albedos at the top of the atmosphere increase as the solar zenith angle increases, or $\partial A_s(a, \theta_0)/\partial\partial_0 > 0$ and $\partial A_c(a, \theta_0, \tau_c)/\partial\theta_0 > 0$, and this is shown in Figs. 3 and 4. The one exception to this relationship is shown in Fig. 3 and occurs for $a > 0.8$ and $\theta_0 > 40°$ when $A_s(a, \theta_0)$ decreases as $\theta_0$ increases. This effect begins to occur for $\theta_0 > 50°$ and $a = 0.65$ as is shown in Table 2. This is because given the two competing effects of $A_s(0, \theta_0)$ increasing and $m_s(\theta_0)$ decreasing as $\theta_0$ increases, the latter effect dominates for large enough a and $\theta_0$ to cause

$$\frac{\partial A_s(a,\theta_0)}{\partial\theta_0} = \left[\frac{\partial m_s(\theta_0)}{\partial\theta_0} a + \frac{\partial A_s(0,\theta_0)}{\partial\theta_0}\right] < 0$$

for this small range of a and $\theta_0$. In this case, the large surface albedo ($a > 0.8$) is a major cause of the large albedo at the top of the atmosphere $A_s(a, \theta_0)$ so that as $\theta_0$ increases beyond 40° less radiation reaches the surrace to take advantage of its effect. This results in the albedo at the top of the atmosphere decreasing as the effect of the surface albedo decreases with increasing $\theta_0$.

In Fig. 3 it was observed by Jacobowitz (1978) that for a surface albedo of approximately 0.75 the dependence of $A_s(a, \theta_0)$ on $\theta_0$ is minimal. This feature could be used in calibrating aircraft or satellite instruments over areas such as White Sands, New Mexico. For example, if we had a three satellite system measuring albedo in the morning, noon, and afternoon as proposed by Woerner (1978) for the Earth Radiation Budget Satellite System (ERBSS) this independence on $\theta_0$ would allow good data comparison for the cloud free data.

Equation 1 has the property that it may be inverted to give the surface albedo in terms of the albedo at the top of the atmosphere:

$$a(A_{meas.}, \theta_0) = [A_{meas.}(\theta_0) - A_s(0, \theta_0)] / m_s(\theta_0) \tag{9}$$

Thus, given a cloud free scene and the measured albedo $A_{meas}(\theta_0)$, one can solve for the spatially averaged surface albedo in the field of view of the measurement by using Eqs. 5 and 7 to compute the intercept and slope functions, respectively. In principle, Eq. 2 could also be inverted to supply surface albedo for cloud obscured fields of view. In practice, except for moderate to high resolution radiometers, it is difficult to find fields of view which are uniform in their atmospheric properties. As a result of variability in the physical characteristics of atmospheric aerosols, such as optical thickness, scattering phase function and single scatter albedo, Eq. 9 does not exactly model all atmospheric variability accurately enough to permit formation of detailed determinations of surface albedo. However, with a relaxation of the accuracy requirements for

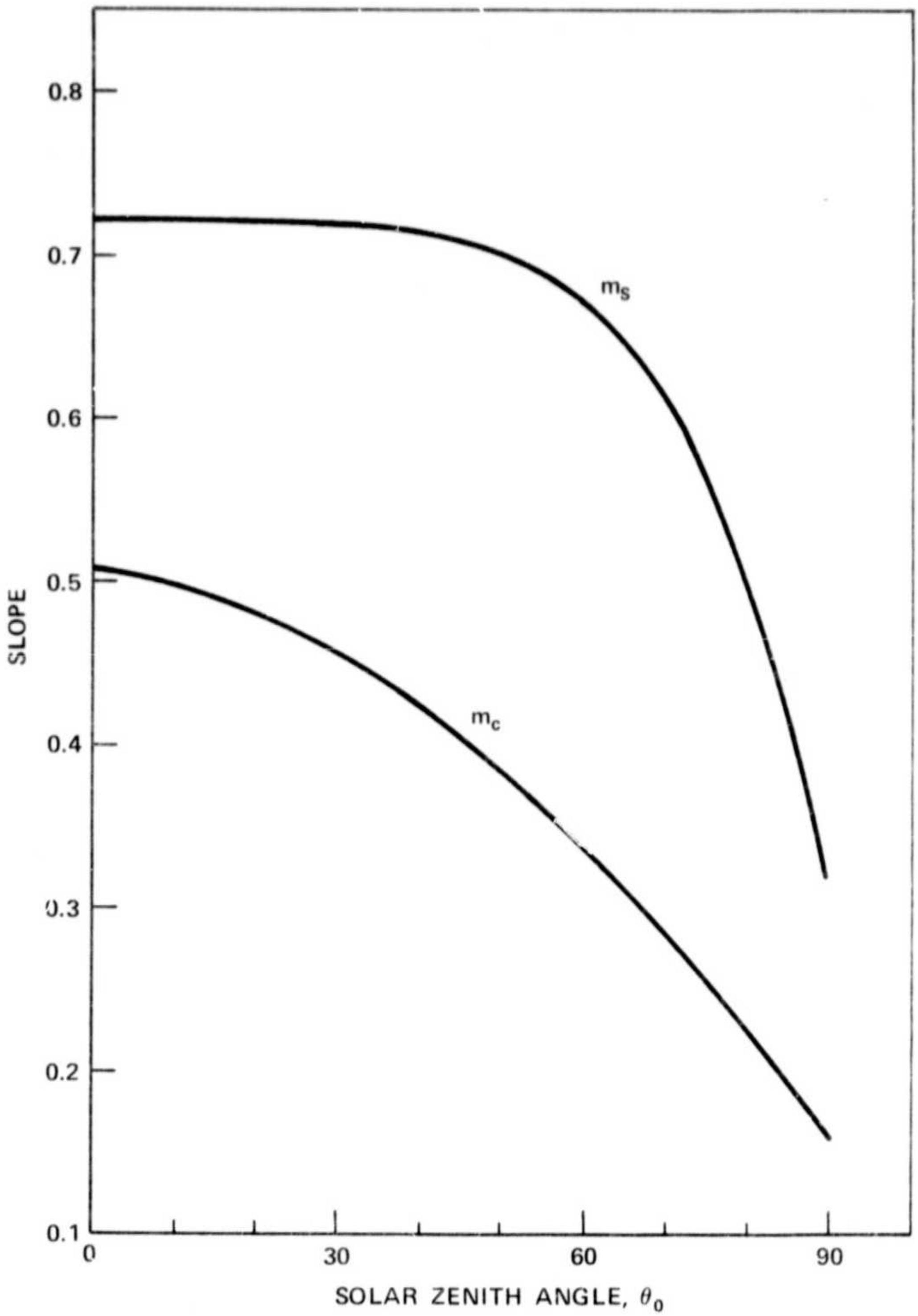


Figure 2. Solar Zenith Angle Dependence of Slope Functions

Table 2

Albedo at the Top of the Cloud Free Atmosphere as a Function of Surface Albedo, a, and Solar Zenith Angle, $\theta_0$

$\theta_0$ (degrees)

| a | 0 | 10 | 20 | 30 | 40 | 50 | 60 | 70 | 80 | 90 |
|---|---|---|---|---|---|---|---|---|---|---|
| 0.00 | 0.0483 | 0.0494 | 0.0523 | 0.0568 | 0.0628 | 0.0722 | 0.0903 | 0.1280 | 0.2046 | 0.3509 |
| 0.05 | 0.0844 | 0.0854 | 0.0884 | 0.0927 | 0.0985 | 0.1072 | 0.1238 | 0.1585 | 0.2297 | 0.3666 |
| 0.10 | 0.1204 | 0.1215 | 0.1244 | 0.1287 | 0.1342 | 0.1422 | 0.1573 | 0.1891 | 0.2549 | 0.3824 |
| 0.15 | 0.1565 | 0.1576 | 0.1605 | 0.1647 | 0.1698 | 0.1772 | 0.1908 | 0.2196 | 0.2800 | 0.3982 |
| 0.20 | 0.1926 | 0.1936 | 0.1965 | 0.2006 | 0.2055 | 0.2122 | 0.2243 | 0.2502 | 0.3051 | 0.4140 |
| 0.25 | 0.2286 | 0.2297 | 0.2326 | 0.2366 | 0.2412 | 0.2472 | 0.2578 | 0.2807 | 0.3302 | 0.4298 |
| 0.30 | 0.2647 | 0.2657 | 0.2686 | 0.2725 | 0.2769 | 0.2822 | 0.2913 | 0.3113 | 0.3554 | 0.4456 |
| 0.35 | 0.3008 | 0.3018 | 0.3047 | 0.3085 | 0.3126 | 0.3172 | 0.3248 | 0.3418 | 0.3805 | 0.4614 |
| 0.40 | 0.3368 | 0.3379 | 0.3407 | 0.3444 | 0.3483 | 0.3522 | 0.3583 | 0.3723 | 0.4056 | 0.4771 |
| 0.45 | 0.3729 | 0.3739 | 0.3768 | 0.3804 | 0.3839 | 0.3872 | 0.3918 | 0.4029 | 0.4307 | 0.4929 |
| 0.50 | 0.4090 | 0.4100 | 0.4128 | 0.4164 | 0.4196 | 0.4222 | 0.4253 | 0.4334 | 0.4558 | 0.5087 |

Table 2 (Continued)

$\theta_0$ (degrees)

| a | 0 | 10 | 20 | 30 | 40 | 50 | 60 | 70 | 80 | 90 |
|---|---|---|---|---|---|---|---|---|---|---|
| 0.55 | 0.4450 | 0.4461 | 0.4488 | 0.4523 | 0.4553 | 0.4572 | 0.4588 | 0.4640 | 0.4810 | 0.5245 |
| 0.60 | 0.4811 | 0.4821 | 0.4849 | 0.4883 | 0.4910 | 0.4922 | 0.4923 | 0.4945 | 0.5061 | 0.5403 |
| 0.65 | 0.5171 | 0.5182 | 0.5209 | 0.5242 | 0.5267 | 0.5272 | 0.5258 | 0.5250 | 0.5312 | 0.5561 |
| 0.70 | 0.5532 | 0.5543 | 0.5570 | 0.5602 | 0.5624 | 0.5622 | 0.5593 | 0.5556 | 0.5563 | 0.5718 |
| 0.75 | 0.5893 | 0.5903 | 0.5930 | 0.5962 | 0.5981 | 0.5972 | 0.5928 | 0.5861 | 0.5815 | 0.5876 |
| 0.80 | 0.6253 | 0.6264 | 0.6291 | 0.6321 | 0.6337 | 0.6322 | 0.6263 | 0.6167 | 0.6066 | 0.6034 |
| 0.85 | 0.6614 | 0.6625 | 0.6651 | 0.6681 | 0.6694 | 0.6672 | 0.6598 | 0.6472 | 0.6317 | 0.6192 |
| 0.90 | 0.6975 | 0.6985 | 0.7012 | 0.7040 | 0.7051 | 0.7022 | 0.6933 | 0.6777 | 0.6568 | 0.6350 |
| 0.95 | 0.7335 | 0.7346 | 0.7372 | 0.7400 | 0.7408 | 0.7372 | 0.7268 | 0.7083 | 0.6820 | 0.6508 |
| 1.00 | 0.7696 | 0.7706 | 0.7733 | 0.7760 | 0.7765 | 0.7721 | 0.7603 | 0.7388 | 0.7071 | 0.6665 |

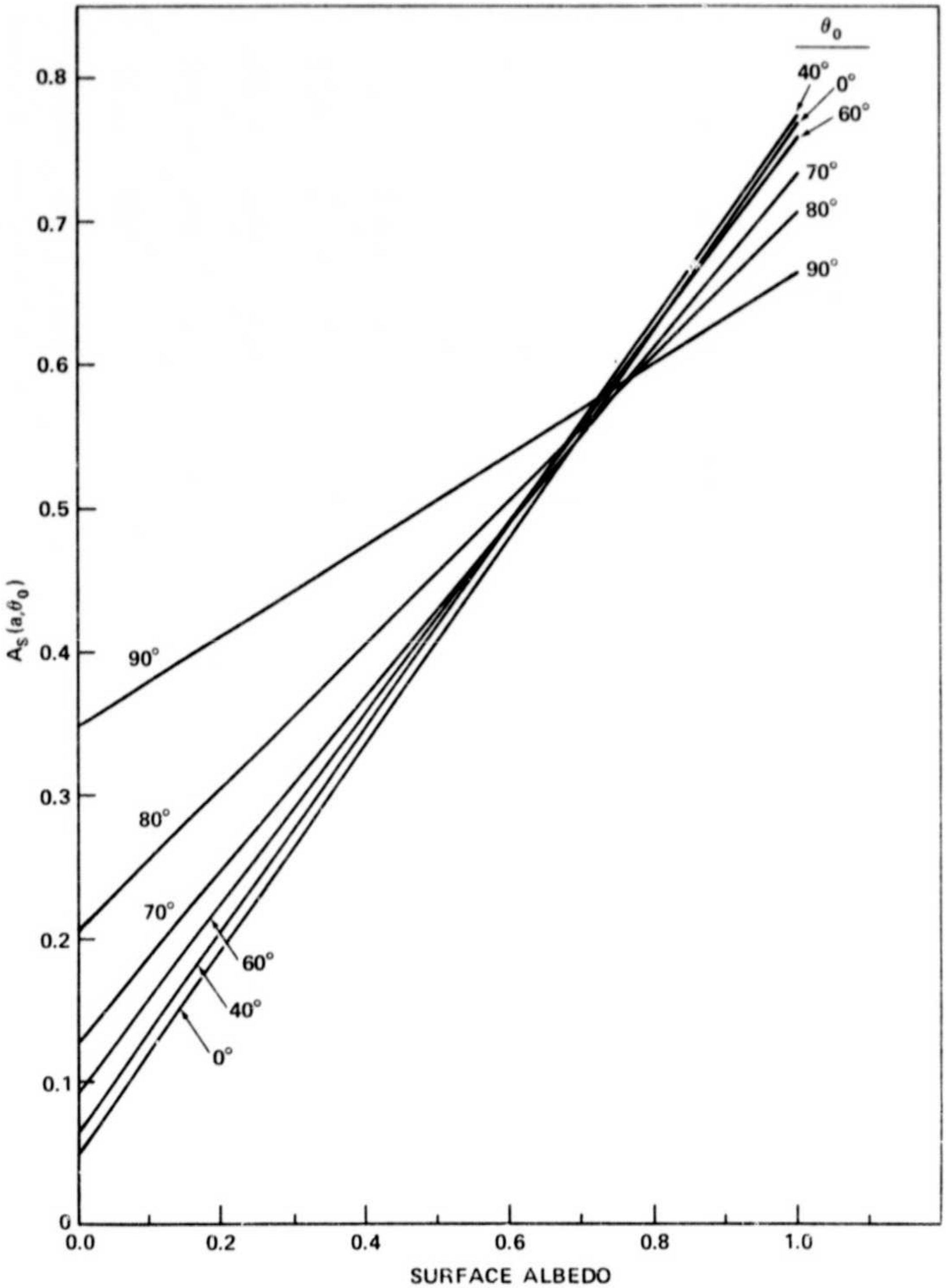


Figure 3. Albedo at the Top of the Cloud-free Atmosphere as a Function of Surface Albedo and for Several Solar Zenith Angles.

Table 3

Albedo at the Top of the Cloudy Atmosphere as a Function of Surface Albedo, a, and Solar Zenith Angle, with the Cloud Optical Thickness $\tau_c$, Contained in the Input Parameter $A_c$ $(0,\ 0,\ \tau_c) = 0.194$

$\theta_0$ (degrees)

| a | 0 | 10 | 20 | 30 | 40 | 50 | 60 | 70 | 80 | 90 |
|---|---|---|---|---|---|---|---|---|---|---|
| 0. 00 | 0. 1940 | 0. 1989 | 0. 2136 | 0. 2382 | 0. 2725 | 0. 3167 | 0. 3706 | 0. 4344 | 0. 5080 | 0. 5914 |
| 0. 05 | 0. 2194 | 0. 2238 | 0. 2376 | 0. 2610 | 0. 2937 | 0. 3359 | 0. 3876 | 0. 4487 | 0. 5193 | 0. 5994 |
| 0. 10 | 0. 2448 | 0. 2487 | 0. 2617 | 0. 2838 | 0. 3149 | 0. 3552 | 0. 4046 | 0. 4631 | 0. 5307 | 0. 6074 |
| 0. 15 | 0. 2702 | 0. 2736 | 0. 2857 | 0. 3066 | 0. 3362 | 0. 3745 | 0. 4216 | 0. 4775 | 0. 5420 | 0. 6154 |
| 0. 20 | 0. 2956 | 0. 2985 | 0. 3097 | 0. 3294 | 0. 3574 | 0. 3938 | 0. 4386 | 0. 4918 | 0. 5534 | 0. 6233 |
| 0. 25 | 0. 3210 | 0. 3233 | 0. 3337 | 0. 3522 | 0. 3786 | 0. 4131 | 0. 4556 | 0. 5062 | 0. 5647 | 0. 6313 |
| 0. 30 | 0. 3464 | 0. 3482 | 0. 3578 | 0. 3750 | 0. 3998 | 0. 4324 | 0. 4726 | 0. 5205 | 0. 5761 | 0. 6393 |
| 0. 35 | 0. 3718 | 0. 3731 | 0. 3818 | 0. 3978 | 0. 4211 | 0. 4517 | 0. 4896 | 0. 5349 | 0. 5874 | 0. 6473 |
| 0. 40 | 0. 3972 | 0. 3980 | 0. 4058 | 0. 4206 | 0. 4423 | 0. 4710 | 0. 5066 | 0. 5492 | 0. 5988 | 0. 6553 |
| 0. 45 | 0. 4226 | 0. 4229 | 0. 4298 | 0. 4434 | 0. 4635 | 0. 4903 | 0. 5236 | 0. 5636 | 0. 6101 | 0. 6633 |
| 0. 50 | 0. 4480 | 0. 4478 | 0. 4538 | 0. 4662 | 0. 4847 | 0. 5095 | 0. 5406 | 0. 5779 | 0. 6215 | 0. 6713 |

Table 3 (Continued)

| a | 0 | 10 | 20 | 30 | 40 | 50 | 60 | 70 | 80 | 90 |
|---|---|---|---|---|---|---|---|---|---|---|
| 0. 55 | 0. 4733 | 0. 4727 | 0. 4779 | 0. 4890 | 0. 5060 | 0. 5288 | 0. 5576 | 0. 5923 | 0. 6328 | 0. 6793 |
| 0. 60 | 0. 4987 | 0. 4975 | 0. 5019 | 0. 5118 | 0. 5272 | 0. 5481 | 0. 5746 | 0. 6066 | 0. 6442 | 0. 6872 |
| 0. 65 | 0. 5241 | 0. 5224 | 0. 5259 | 0. 5346 | 0. 5484 | 0. 5674 | 0. 5916 | 0. 6210 | 0. 6555 | 0. 6952 |
| 0. 70 | 0. 5495 | 0. 5473 | 0. 5499 | 0. 5574 | 0. 5696 | 0. 5867 | 0. 6086 | 0. 6353 | 0. 6669 | 0. 7032 |
| 0. 75 | 0. 5749 | 0. 5722 | 0. 5740 | 0. 5802 | 0. 5909 | 0. 6060 | 0. 6256 | 0. 6497 | 0. 6782 | 0. 7112 |
| 0. 80 | 0. 6003 | 0. 5971 | 0. 5980 | 0. 6030 | 0. 6121 | 0. 6253 | 0. 6426 | 0. 6640 | 0. 6896 | 0. 7192 |
| 0. 85 | 0. 6257 | 0. 6220 | 0. 6220 | 0. 6258 | 0. 6333 | 0. 6446 | 0. 6596 | 0. 6784 | 0. 7009 | 0. 7272 |
| 0. 90 | 0. 6511 | 0. 6469 | 0. 6460 | 0. 6486 | 0. 6545 | 0. 6639 | 0. 6766 | 0. 6927 | 0. 7123 | 0. 7352 |
| 0. 95 | 0. 6765 | 0. 6718 | 0. 6700 | 0. 6714 | 0. 6757 | 0. 6832 | 0. 6936 | 0. 7071 | 0. 7236 | 0. 7432 |
| 1. 00 | 0. 7019 | 0. 6966 | 0. 6941 | 0. 6942 | 0. 6970 | 0. 7024 | 0. 7106 | 0. 7214 | 0. 7350 | 0. 7512 |

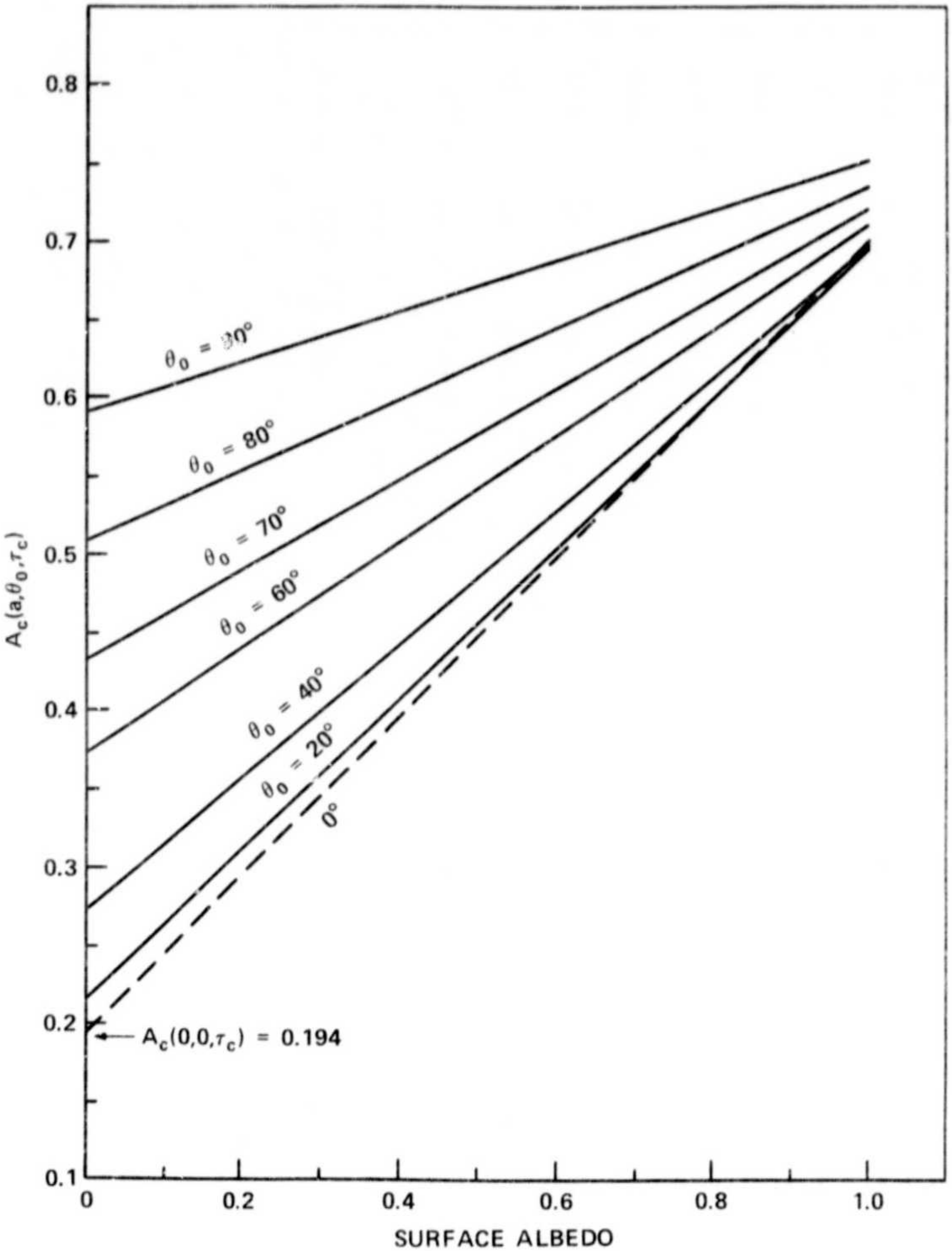


Figure 4. Albedo at the Top of a Cloudy Atmosphere as a Function of Surface Albedo and Solar Zenith Angle

the determination of surface albedo, global maps of surface albedo can be formed using Eq. 9 and satellite determined, high resolution albedos.

## 3. TRANSFORMATION FOR GENERALIZED CLOUDY ATMOSPHERE

As noted in Section 2 both the slope and intercept functions of Eq. 2 should depend on the cloud layer optical depth by being explicitly dependent on $\tau_c$ or implicitly dependent on $\tau_c$ through a dependence on $A_c(0, 0, \tau_c)$. We in general use the latter dependency.

The intercept dependency of $A_c(0, \theta_0, \tau_c)$ on $A_c(0, 0, \tau_c)$ is shown in Eq. 6. Using this equation we compute values for $A_c(0, \theta_0, \tau_c)$ for input values of $A_c(0, 0, \tau_c) = 0.1940, 0.2091, 0.30, 0.40, 0.45, 0.50, 0.55$, and $0.60$, and these results are shown in Table 4 and Figure 5. The values of $A_c(0, \theta_0, \tau_c)$ computed for $A_c(0, 0, \tau_c) = 0.2091$ are in close agreement with the D1-ST results of Table 4 from DB (1974), even though the increase in optical depth in this atmospheric model is due to the aerosol distribution and not the cloud layer.

The dependency of the slope function on $\tau_c$ is contained in the $g(\tau_c)$ function of Eq. 3.

We now use this implicit dependency on $\tau_c$ of $A_c(a, \theta_0, \tau_c)$ through $A_c(0, 0, \tau_c)$ to compute $A_c(a, \theta_0, \tau_c)$ for different values of a and $\theta_0$. These results are shown in Table 5 and Figure 6 for $A_c(0, 0, \tau_c) = 0.50$. We again see that the albedo at the top of the atmosphere has a very weak

Table 4

Cloud Albedos, $A_c$ $(0, \theta_0, \tau_c)$

| | $A_c$ $(0, 0, \tau_c)$ | | | | | | | |
|---|---|---|---|---|---|---|---|---|
| $\theta_0$ | 0.19 | 0.21 | 0.30 | 0.40 | 0.45 | 0.50 | 0.55 | 0.60 |
| 0 | 0.19 | 0.21 | 0.30 | 0.40 | 0.45 | 0.50 | 0.55 | 0.60 |
| 5 | 0.19 | 0.21 | 0.30 | 0.40 | 0.45 | 0.50 | 0.55 | 0.60 |
| 10 | 0.19 | 0.21 | 0.30 | 0.40 | 0.45 | 0.50 | 0.55 | 0.60 |
| 15 | 0.20 | 0.22 | 0.31 | 0.41 | 0.46 | 0.51 | 0.56 | 0.61 |
| 20 | 0.21 | 0.23 | 0.32 | 0.42 | 0.47 | 0.52 | 0.57 | 0.62 |
| 25 | 0.22 | 0.24 | 0.33 | 0.43 | 0.48 | 0.53 | 0.58 | 0.63 |
| 30 | 0.23 | 0.25 | 0.34 | 0.44 | 0.49 | 0.54 | 0.59 | 0.64 |
| 35 | 0.25 | 0.27 | 0.36 | 0.46 | 0.51 | 0.56 | 0.61 | 0.66 |
| 40 | 0.27 | 0.29 | 0.38 | 0.48 | 0.53 | 0.58 | 0.63 | 0.68 |
| 45 | 0.29 | 0.31 | 0.40 | 0.50 | 0.55 | 0.60 | 0.65 | 0.70 |
| 50 | 0.31 | 0.33 | 0.42 | 0.52 | 0.57 | 0.62 | 0.67 | 0.72 |
| 55 | 0.34 | 0.36 | 0.45 | 0.55 | 0.60 | 0.65 | 0.70 | 0.75 |
| 60 | 0.37 | 0.39 | 0.48 | 0.58 | 0.63 | 0.68 | 0.73 | 0.78 |
| 65 | 0.40 | 0.42 | 0.51 | 0.61 | 0.66 | 0.71 | 0.76 | 0.81 |
| 70 | 0.43 | 0.45 | 0.54 | 0.64 | 0.69 | 0.74 | 0.79 | 0.84 |
| 75 | 0.47 | 0.49 | 0.58 | 0.68 | 0.73 | 0.78 | 0.83 | 0.88 |
| 80 | 0.50 | 0.52 | 0.61 | 0.71 | 0.76 | 0.81 | 0.86 | 0.91 |
| 85 | 0.54 | 0.56 | 0.65 | 0.75 | 0.80 | 0.85 | 0.90 | 0.95 |
| 90 | 0.59 | 0.61 | 0.70 | 0.80 | 0.85 | 0.90 | 0.95 | 1.00 |

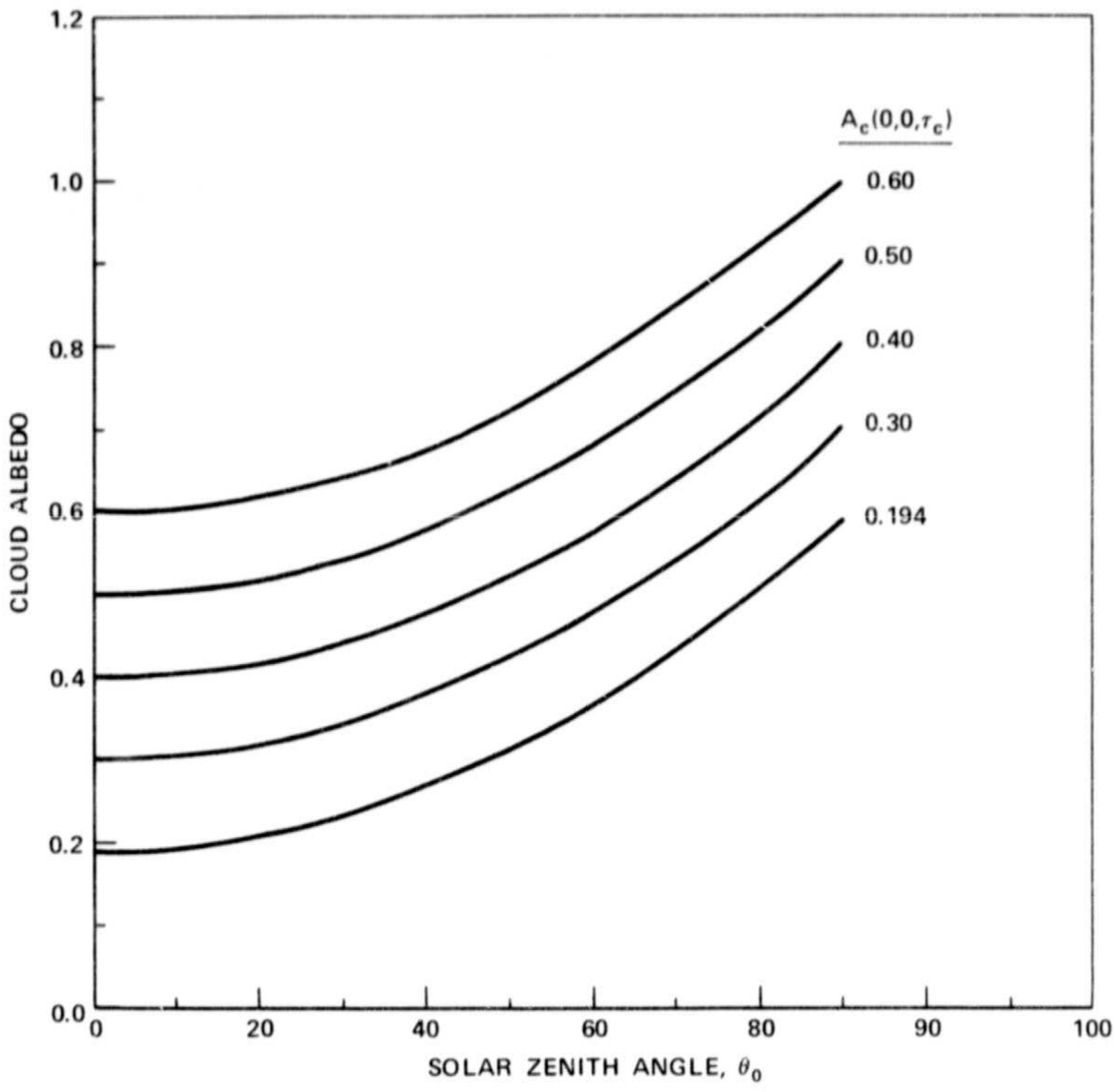


Figure 5. Cloud Albedos as a Function of Solar Zenith Angle for the Five Different Intercept Values $A_c$ $(0,\ 0,\ \tau_c)$ of Table 4.

Table 5

Albedo, $A_c$ (a, $\theta_0$, $\tau_c$), at the Top of The Cloudy Atmosphere as a Function of Surface Albedo, a and Solar Zenith Angle, $\theta_0$, with the Cloud Optical Thickness, $\tau_c$, Contained in the Input Parameter

$A_c$ (0, 0, $\tau_c$) = 0. 5.

$\theta_0$ (degrees)

| a | 0 | 10 | 20 | 30 | 40 | 50 | 60 | 70 | 80 | 90 |
|---|---|---|---|---|---|---|---|---|---|---|
| 0. 00 | 0. 5000 | 0. 5049 | 0. 5196 | 0. 5442 | 0. 5785 | 0. 6227 | 0. 6766 | 0. 7404 | 0. 8140 | 0. 8974 |
| 0. 05 | 0. 5099 | 0. 5146 | 0. 5289 | 0. 5530 | 0. 5867 | 0. 6301 | 0. 6832 | 0. 7460 | 0. 8184 | 0. 9005 |
| 0. 10 | 0. 5197 | 0. 5242 | 0. 5383 | 0. 5618 | 0. 5950 | 0. 6376 | 0. 6898 | 0. 7515 | 0. 8228 | 0. 9036 |
| 0. 15 | 0. 5296 | 0. 5339 | 0. 5476 | 0. 5707 | 0. 6032 | 0. 6451 | 0. 6964 | 0. 7571 | 0. 8272 | 0. 9067 |
| 0. 20 | 0. 5394 | 0. 5435 | 0. 5569 | 0. 5795 | 0. 6114 | 0. 6526 | 0. 7030 | 0. 7627 | 0. 8316 | 0. 9098 |
| 0. 25 | 0. 5493 | 0. 5532 | 0. 5662 | 0. 5884 | 0. 6197 | 0. 6601 | 0. 7096 | 0. 7682 | 0. 8360 | 0. 9129 |
| 0. 30 | 0. 5591 | 0. 5628 | 0. 5755 | 0. 5972 | 0. 6279 | 0. 6676 | 0. 7162 | 0. 7738 | 0. 8404 | 0. 9160 |
| 0. 35 | 0. 5690 | 0. 5725 | 0. 5849 | 0. 6061 | 0. 6361 | 0. 6750 | 0. 7228 | 0. 7794 | 0. 8448 | 0. 9191 |
| 0. 40 | 0. 5788 | 0. 5822 | 0. 5942 | 0. 6149 | 0. 6444 | 0. 6825 | 0. 7294 | 0. 7849 | 0. 8492 | 0. 9222 |
| 0. 45 | 0. 5887 | 0. 5918 | 0. 6035 | 0. 6238 | 0. 6526 | 0. 6900 | 0. 7360 | 0. 7905 | 0. 8536 | 0. 9253 |
| 0. 50 | 0. 5985 | 0. 6015 | 0. 6128 | 0. 6326 | 0. 6608 | 0. 6975 | 0. 7426 | 0. 7961 | 0. 8580 | 0. 9284 |

Table 5 (Continued)

| a | 0 | 10 | 20 | 30 | 40 | 50 | 60 | 70 | 80 | 90 |
|---|---|---|---|---|---|---|---|---|---|---|
| 0.55 | 0.6084 | 0.6111 | 0.6222 | 0.6415 | 0.6691 | 0.7050 | 0.7492 | 0.8016 | 0.8624 | 0.9315 |
| 0.60 | 0.6182 | 0.6208 | 0.6315 | 0.6503 | 0.6773 | 0.7125 | 0.7558 | 0.8072 | 0.8668 | 0.9346 |
| 0.65 | 0.6281 | 0.6304 | 0.6408 | 0.6592 | 0.6855 | 0.7199 | 0.7624 | 0.8128 | 0.8712 | 0.9377 |
| 0.70 | 0.6379 | 0.6401 | 0.6501 | 0.6680 | 0.6938 | 0.7274 | 0.7690 | 0.8184 | 0.8756 | 0.9408 |
| 0.75 | 0.6478 | 0.6497 | 0.6594 | 0.6769 | 0.7020 | 0.7349 | 0.7756 | 0.8239 | 0.8800 | 0.9439 |
| 0.80 | 0.6577 | 0.6594 | 0.6688 | 0.6857 | 0.7103 | 0.7424 | 0.7821 | 0.8295 | 0.8844 | 0.9470 |
| 0.85 | 0.6675 | 0.6691 | 0.6781 | 0.6946 | 0.7185 | 0.7499 | 0.7887 | 0.8351 | 0.8888 | 0.9501 |
| 0.90 | 0.6774 | 0.6787 | 0.6874 | 0.7034 | 0.7267 | 0.7574 | 0.7953 | 0.8406 | 0.8932 | 0.9532 |
| 0.95 | 0.6872 | 0.6884 | 0.6967 | 0.7122 | 0.7350 | 0.7649 | 0.8019 | 0.8462 | 0.8976 | 0.9563 |
| 1.00 | 0.6971 | 0.6980 | 0.7060 | 0.7211 | 0.7432 | 0.7723 | 0.8085 | 0.8518 | 0.9020 | 0.9594 |

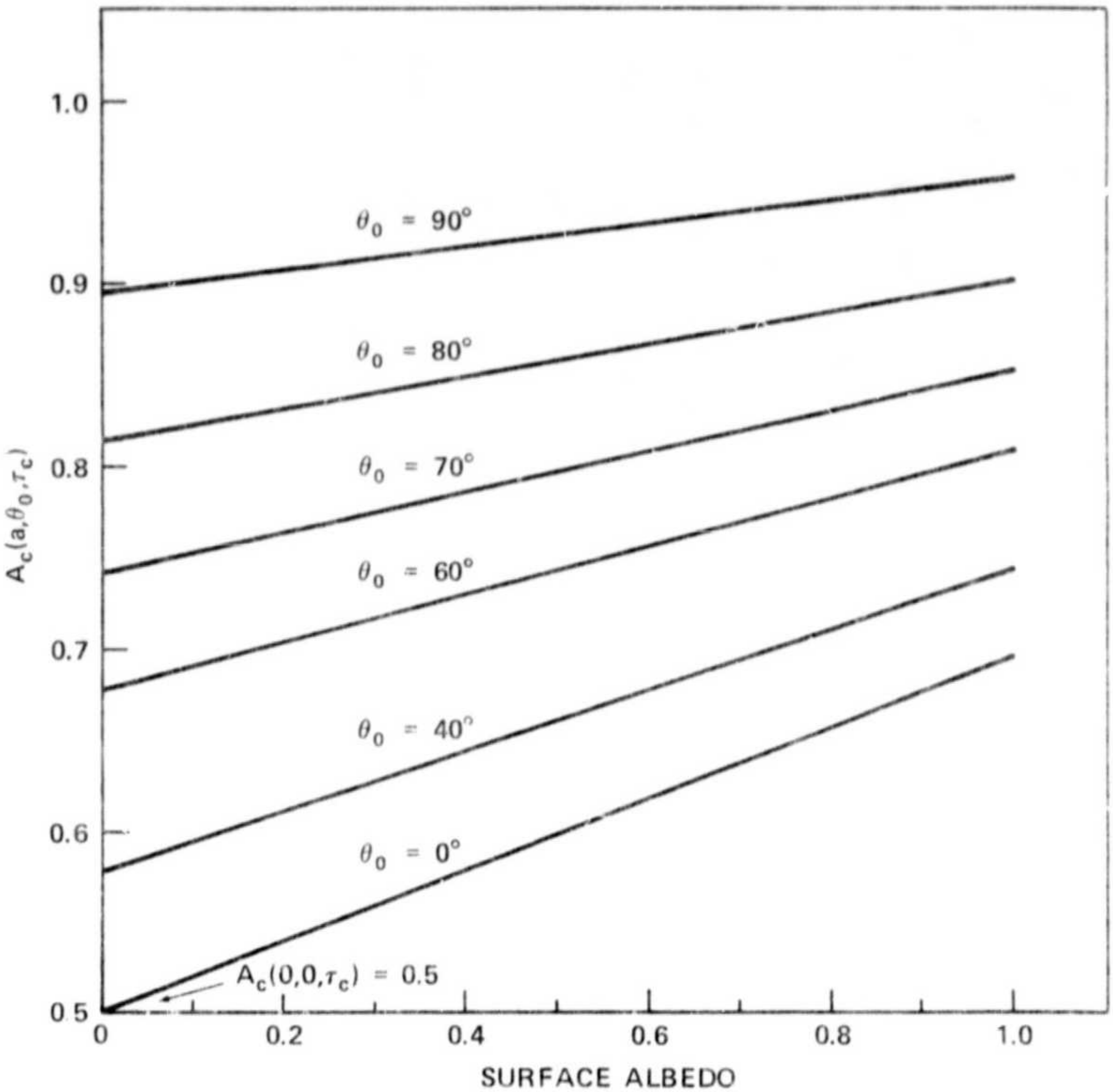


Figure 6. Albedo at the Top of a Cloudy Atmosphere as a Function of Surface Albedo and Solar Zenith Angle

dependence on surface albedo for large solar zenith angles; e.g. $A_c(a, 90, \tau_c)$ increases only 6.7% when a increases from 0.0 to 1.0 We also see that in general a comparison between Tables 5 and 2 shows that $A_c > A_s$, except for values below the discriminator line in Table 5 when $A_s(a, \theta_0) > A_c(a, \theta_0, \tau_c)$. The reasons for this effect are discussed in Section 2. We see that the range of values of a and $\theta_0$ when $A_s > A_c$ are now decreased with an increase in the cloud optical thickness, when $A_c(0, 0, \tau_c)$ increases from 0.194 in Table 3 to 0.50 in Table 5.

## 4. SPATIAL RESOLUTION AND FRACTIONAL SURFACE AND CLOUD COVER

A general measurement of albedo at the top of the atmosphere occurs during conditions when a fraction of the field of view (FOV) of the instrument is covered by clouds ($f_c$) and a fraction of the surface in the FOV is covered by an albedo $a_k$, where the fractions ($f_k$) of the k = 1, N types of surfaces satisfy

$$1 = \sum_{k=1}^{N} f_k . \tag{10}$$

We will assume that the surface albedo in the FOV can be expressed by

$$a = \sum_{k=1}^{N} f_k a_k . \tag{11}$$

The application of our cloud free ($A_s$) and total cloud cover ($A_c$) albedos to the analysis of albedo data (A) with fractional cloud cover will now be presented for the cases of high and low spatial resolution albedo data. We will assume we have this data at time t, with a solar zenith angle $\theta_0$ (t), over an average surface albedo a obtained from Eq. 11. The cases we discuss are high and low resolution data, fractional cloud cover with random and known distributions over the FOV, and data for these values of a, $\theta_0$, and t averaged over a time period T.

If we have high spatial resolution data so that the surface in the FOV can be characterized by a single value of surface albedo and the size of the FOV allows a yes or no cloud decision then the albedo A for a given picture element (pixel) can be used to classify that pixel using the following tests;

| Test | Class of Pixel |
|---|---|
| $A < A_s (a, \theta_0)$ | cloud free, low aerosols |
| $A_s (a, \theta_0) \leqslant A \leqslant A_c (a, \theta_0, \tau_c)$ | cloud free, heavy aerosols, or small clouds |
| $A_c (a, \theta_0, \tau_c) < A$ | cloud |

where $A_c$ $(0, 0, \tau_c) = 0.20$, for example, could be used to compute $A_c$ $(a, \theta_0, \tau_c)$ for our lower cloud threshold in this test. The cloud pixels could be further divided into low, medium, or high albedo (or optical thickness) clouds if additional tests on A using selected ranges of (0.20, 0.35), (0.35, 0.50), and >0.50 for $A_c$ $(0, 0, \tau_c)$ were used to compute test ranges of $A_c$ $(a, \theta_0, \tau_c)$.

If we have low spatial resolution data where clouds of characteristic optical thickness $\tau_c$ or albedo $A_c$ $(0, 0, \tau_c)$ in general fill a fraction $f_c$ of the FOV then the explicit albedo dependence on our variables can be expressed by

$$A = A(a, \theta_0, \tau_c, f_c) \tag{12}$$

A simplified way of representing the dependence of A on $(a, \theta_0, \tau_c)$ implicitly is given by

$$A = A(A_s, A_c, f_c) = A[A_s(a, \theta_0), A_c(a, \theta_0, \tau_c), f_c]. \tag{13}$$

If we assume the form of Eq. 13 is valid then a polynomial in $f_c$ of the form

$$A = \sum_{n=0}^{M} \alpha_n f_c^n \tag{14}$$

$$\alpha_n = \alpha_n(A_s, A_c) = \alpha_n [A_s(a, \theta_0), A_c(a, \theta_0, \tau_c)] \tag{15}$$

is one way of approximating A. If the value of $A_c$ $(0, 0, \tau_c)$ selected to characterize our typical cloud causes $A_c$ $(a, \theta_0, \tau_c)$ to be an upper limit to the measured values of A then three constraints which could be used to determine $\alpha_n$ are

$$A = A_s \qquad \text{if} \qquad f_c = 0, \tag{16}$$

$$A = A_c \qquad \text{if} \qquad f_c = 1, \tag{17}$$

$$A_s < A < A_c \qquad \text{if} \qquad 0 < f_c < 1. \tag{18}$$

The Monte Carlo results of Davis, Cox, and McKee (1978) for finite and infinite cloud layers support the decrease in A of Eq. 18 for $f_c < 1$. In Fig. 7

we schematically show the two endpoints of A determined by Eqs. 16 and 17, and a linear and two quadratic examples of Eq. 14. For the linear case of Eq. 14 the constraints of Eqs. 16 and 17 determine the solution

$$\alpha_0 = A_s , \tag{19}$$

$$\alpha_1 = A_c - A_s , \tag{20}$$

$$A = A_s + (A_c - A_s) f_c = (1 - f_c) A_s + f_c A_c . \tag{21}$$

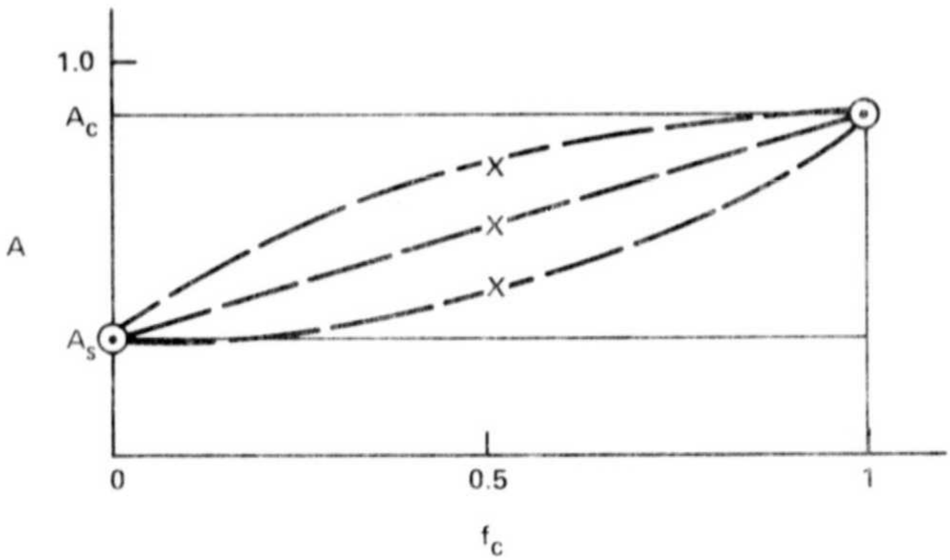


Figure 7. Schematic Relationships Between Measured Albedo and Cloud Fraction

This equation is identical to Eq. 2.90 of Budyko (1974), and similar to Eqs. 12, 17, 18, and 19 of Nack and Green (1974) who characterized fluxes reaching the ground in this manner. For $f_c = 1/2$ in Eq. 21 we have $A = 1/2\ (A_s + A_c)$. If some technique could determine the value of A for $f_c = 1/2$, or $A\ (A_s , A_c , 1/2)$, then this value could be used to determine the following solution to the quadratic case of Eq. 14;

$$\alpha_0 = A_s, \tag{22}$$

$$\alpha_1 = 4A(A_s, A_c, \tfrac{1}{2}) - 3A_s - A_c, \tag{23}$$

$$\alpha_2 = 2(A_s + A_c) - 4A(A_s, A_c, \tfrac{1}{2}), \tag{24}$$

$$\begin{aligned} A = A_s &+ [4A(A_s, A_c, \tfrac{1}{2}) - 3A_s - A_c]\, f_c \\ &+ 2[A_s + A_c - 2A(A_s, A_c, \tfrac{1}{2})]\, f_c^2. \end{aligned} \tag{25}$$

When A $(A_s, A_c, 1/2\ (A_s + A_c)$ this quadratic relationship degenerates to the linear relationship of Eq. 21.

We note that the constraints of Eqs. 16 and 17 are always valid, but that for a small range of (a, $\theta_0$) the relationship $A_s > A_c$ can hold as is discussed in Sections 2 and 3. When this occurs we must interchange $A_s$ with $A_c$ in Eqs. 18 to 25 and Fig. 7. Since the work of CWN(78) uses values of $A_c$ close to those of Table 5 and values of a $\leqslant 0.75$ the problem of $A_s > A_c$ will not arise, and will not be discussed further.

A technique which could be used to compute values of A for different values of $f_c$, such as A $(A_s, A_c, 1/2)$, is the Monte Carlo computer simulation of radiative transfer through an atmosphere with fractional cloud cover. These values of A for different values of $f_c$ could then be used to determine higher order values of $\alpha_n$. Due to the lengthy computer time requirements of such a program it might initially be run for just one characteristic wavelength and for a single typical set of values of a, $\theta_0$, and $\tau_c$ using a single random cloud distribution over the FOV.

If auxiliary information was available which gave the spatial distribution of the clouds over the FOV then the appropriate surface albedos should be used in Eq. 13. For example, if the surface in the FOV is half ice and half water with albedos $a_I = 0.7$ and $a_W = 0.1$ for the ice and water, then in general the albedos for the cases (1) clouds only over ice, (2) clouds only over water, or (3) clouds randomly distributed over ice and water for $f_c = 1/2$ are all unequal;

$$\begin{aligned} A_1 [A_s(a_W, \theta_0), A_c(a_I, \theta_0, \tau_c), \tfrac{1}{2}] &\neq A_2 [A_s(a_I, \theta_0), A_c(a_W, \theta_0, \tau_c), \tfrac{1}{2}] \\ &\neq A_3 [A_s(a, \theta_0), A_c(a, \theta_0, \tau_c), \tfrac{1}{2}] \end{aligned} \tag{26}$$

where $a = 1/2\ (a_I + a_W) = 0.4$ using Eq. 11.

If at a given time both low and high spatial resolution albedo data were available then the fraction of high resolution pixels classified as clouds of all the pixels in the low resolution FOV could be used as the truth value of $f_c$. This truth value could be compared with the determination of $f_c$ from the low resolution data found by solving, for example, Eq. 21 for $f_c$, or

$$f_c = (A - A_s) / (A_c - A_s). \tag{27}$$

If we have low resolution albedo data averaged over a time period T for the same values of (a, $\theta_0$) then the time averaged albedo data $\overline{A}$ could be expressed in terms of the time averaged fractional cloud cover $\bar{f}_c$ using Eq. 14 in general, or for example Eq. 21 as follows;

$$\bar{A}[A_s, A_c, \bar{f}_c(\theta_0)] = [1 - \bar{f}_c(\theta_0)] A_s + \bar{f}_c(\theta_0) A_c. \tag{28}$$

The temporal averaging of high resolution albedo data involves direct averaging of the results of the cloud or no cloud decision for a given pixel over the period T.

## 5. ALBEDO DEFINITION, REFLECTED IRRADIANCE, AND SPECTRAL AND TEMPORAL AVERAGES

The albedo of the earth-atmosphere system A is the ratio of the reflected irradiance $W_R$ over the incident solar irradiance $W_0$ at the top of the atmosphere, or $A = W_R/W_0$. In general, the irradiance quantities are of greater significance to studies of the energetics of the atmosphere than albedo. This definition will be applied to the spectral plane albedo $A(\lambda, \theta_0)$, and will determine the weighting functions used to define the spectrally averaged albedo $A(\theta_0)$, and the temporally averaged albedo A, where $\lambda$ is a particular wavelength in the shortwave part of the spectrum used by Dave and Braslau (1974, 1975) and bounded by $\lambda_1 = 0.285$ $\mu$m and $\lambda_2 = 2.5$ $\mu$m. The solar zenith angle $\theta_0$ depends on the latitude, the local time t elapsed since noon, and the day of the year. Temporal averaging in general would apply to the $\theta_0(t)$ dependence over a sunlit part of the day during an interval $T = t_2 - t_1$ bounded by $(t_1, t_2)$, and when these bounds are sunrise and sunset a daily average is obtained. The non-weighted spectral $\langle A(\theta_0)\rangle$ and temporal $\langle A\rangle$ albedo averages will also be given, but these do not satisfy our definition of albedo.

The spectrally and temporally integrated reflected irradiances are defined as

$$W_R(\theta_0) = \int_{\lambda_1}^{\lambda_2} W_R(\lambda, \theta_0)\, d\lambda, \tag{29}$$

$$W_R = \frac{1}{(t_2 - t_1)} \int_{t_1}^{t_2} W_R(\theta_0)\, dt. \tag{30}$$

The incident solar radiance

$$I(\lambda, \mu, \phi; \mu_0, \phi_0) = H_0(\lambda)\, \delta(\mu - \mu_0)\, \delta(\phi - \phi_0) \tag{31}$$

traveling in direction $(\mu, \phi)$ with the sun at direction $(\mu_0, \phi_0)$ is related to the incident solar irradiance by

$$\begin{aligned} W_0(\lambda, \theta_0) &= \int_0^1 d\mu \int_0^{2\pi} d\phi\, \mu\, H_0(\lambda)\, \delta(\mu - \mu_0)\, \delta(\phi - \phi_0) \\ &= \mu_0\, H_0(\lambda), \end{aligned} \tag{32}$$

where $\delta$ denotes the Dirac delta function. A direction is specified by $(\mu, \phi)$, where $\mu = \cos\theta$ and $(\theta, \phi)$ are (zenith, azimuth) angles. The solar energy $dE_0$ incident on an area $d\sigma$ over the wavelength and time intervals $d\lambda$ and $dt$ is given by

$$H_0(\lambda) = \frac{dE_0}{dt\, d\sigma\, d\lambda} = W_o(\lambda, 0) \tag{33}$$

The spectrally and temporally integrated incident solar irradiances are given by

$$W_{0S}(\theta_0) = \int_{\lambda_1}^{\lambda_2} W_0(\lambda, \theta_0)\, d\lambda = \mu_0\, H_{0S} \tag{34}$$

$$H_{0S} = \int_{\lambda_1}^{\lambda_2} H_0(\lambda)\, d\lambda = (\lambda_2 - \lambda_1)\, \bar{H}_{0S} \tag{35}$$

$$W_{0S} = \frac{1}{(t_2 - t_1)} \int_{t_1}^{t_2} W_{0S}(\theta_0)\, dt = \bar{\mu}_0 \, H_{0S} \tag{36}$$

$$\bar{\mu}_0 = \frac{1}{(t_2 - t_1)} \int_{t_1}^{t_2} \mu_0 \, dt \tag{37}$$

where $H_{0S}$ is the incident shortwave energy over intervals dt and $d\sigma$, $\bar{H}_{0S}$ is the mean value of $H_{0S}$, $W_{0S}$ is the incident shortwave irradiance over the interval $(t_2 - t_1)$, and $\bar{\mu}_0$ is the mean value of $\mu_0$ over this time interval.

To derive our weighting functions we start with our definition applied to the spectral albedo

$$A(\lambda, \theta_0) = \frac{W_R(\lambda, \theta_0)}{W_0(\lambda, \theta_0)} = \frac{W_R(\lambda, \theta_0)}{\mu_0 H_0(\lambda)}. \tag{38}$$

The weighting function which satisfies our definition for the spectrally averaged albedo

$$\begin{aligned} A(\theta_0) &= \frac{W_R(\theta_0)}{W_{0S}(\theta_0)} = \int_{\lambda_1}^{\lambda_2} \left[ \frac{W_0(\lambda, \theta_0)}{W_{0S}(\theta_0)} \right] \frac{W_R(\lambda, \theta_0)}{W_0(\lambda, \theta_0)} \, d\lambda \\ &= \frac{1}{(\lambda_2 - \lambda_1)} \int_{\lambda_1}^{\lambda_2} \left[ \frac{H_0(\lambda)}{\bar{H}_{0S}} \right] A(\lambda, \theta_0) \, d\lambda \end{aligned} \tag{39}$$

is given by $H_0(\lambda)/\overline{H}_{0S}$, and this is consistent with Eq. 2 of Dave and Braslau (1975). The weighting function which satisfies our definition for the temporally averaged albedo

$$A = \frac{W_R}{W_{0S}} = \frac{1}{(t_2 - t_1)} \int_{t_1}^{t_2} \left[\frac{W_{0S}(\theta_0)}{W_{0S}}\right] \frac{W_R(\theta_0)}{W_{0S}(\theta_0)}\, dt$$
$$= \frac{1}{(t_2 - t_1)} \int_{t_1}^{t_2} \left(\frac{\mu_0}{\bar{\mu}_0}\right) A(\theta_0)\, dt \tag{40}$$

is given by $\mu_0/\bar{\mu}_0$.

The relationships between irradiances and albedos are now

$$W_R(\lambda, \theta_0) = \mu_0 H_0(\lambda) A(\lambda, \theta_0), \tag{41}$$

$$W_R(\theta_0) = \mu_0 H_{0S} A(\theta_0), \tag{42}$$

$$W_R = \bar{\mu}_0 H_{0S} A. \tag{43}$$

If non-weighted spectrally and temporally averaged albedos defined by

$$\langle A(\theta_0)\rangle = \frac{1}{(\lambda_2 - \lambda_1)} \int_{\lambda_1}^{\lambda_2} A(\lambda, \theta_0)\, d\lambda \tag{44}$$

$$\langle A\rangle = \frac{1}{(t_2 - t_1)} \int_{t_1}^{t_2} \langle A(\theta_0)\rangle\, dt \tag{45}$$

are used then they have no simple direct relationship with their corresponding irradiances as in Eqs. 42 and 43.

We can now combine Eqs. 1 through 8 with Eq. 42 to obtain the following transformations of surface albedo to reflected irradiances at the top of clear $W_S$ and cloudy $W_c$ atmospheres;

$$W_S(a, \theta_0) = \mu_0 H_{0S} A_S(a, \theta_0), \tag{46}$$

$$W_c(a, \theta_0, \tau_c) = \mu_0 H_{0S} A_c(a, \theta_0, \tau_c). \tag{47}$$

If we apply Eq. 21 to the fractional cloud cover case we have

$$\begin{aligned} W(a, \theta_0, \tau_c, f_c) &= \mu_0 H_S A(A_S, A_c, f_c) \\ &= (1 - f_c) W_S(a, \theta_0) + f_c W_c(a, \theta_0, \tau_c) \\ &= W(W_S, W_c, f_c), \end{aligned} \tag{48}$$

where in general we expect $\theta_0$, $\tau_c$, and $f_c$ to depend on the time of day t at a given location.

## 6. DAILY AND MONTHLY AVERAGED ALBEDOS AND REFLECTED IRRADIANCES

One of the basic problems in acquiring climatological radiation data from satellite platforms is the temporal sampling problem. A polar orbiting satellite will sample the reflected irradiance which is used to compute albedos at a given time of day for many locations so that global spatial sampling is achieved. A geostationary satellite could sample a given region of the globe with high temporal resolution, so that a costly system of well spaced geostationary satellites could give fine temporal and spatial sampling resolution. We will now show how our $\theta_0(t)$ parameterizations of albedos can be used to overcome the temporal sampling problem of the less costly polar orbiting satellite.

We wish to compute time averages of albedo and reflected irradiance at the top of the atmosphere at a latitude and longitude for an area whose surface albedo, $a_{mj}$, remains constant during the $j^{th}$ day of the $m^{th}$ month. The cloud free and total cloud cover cases will be presented first where $\tau_c$ will be independent of time. The time dependence of the solar zenith angle $\theta_0(t)$ can be computed from a well known equation of astronomy [see p. 50 of Smart (1965)]

$$\theta_0(t) = \cos^{-1} \mu_0(t) \tag{49}$$

$$\mu_0(t) = \sin\delta_{mj} \sin\phi + \cos\delta_{mj} \cos\phi \cos H(t) \tag{50}$$

$$H(t) = 2\pi t/T \tag{51}$$

where $\phi$ is the latitude, $\delta_{mj}$ is the solar declination, T is the earth's rotation period (24 hours), t is the time elapsed since noon, and H is the hour angle. The times of sunrise and sunset, $\pm T_{mj}$, are defined by $\mu_0(t) = 0$ so that Eq. 50 gives us

$$\cos(2\pi T_{mj}/T) = - \tan\delta_{mj} \tan\phi, \tag{52}$$

and the minimum solar zenith angle $\theta_{mj}$ is determined by t = 0 so that

$$\cos\theta_{mj} = \sin\delta_{mj}\sin\phi + \cos\delta_{mj}\cos\phi = \cos(\phi - \delta_{mj}). \tag{53}$$

$$\theta_{mj} = \phi - \delta_{mj}. \tag{54}$$

If we let $(t_1, t_2) = (-T_{mj}, T_{mj})$ in Eq. 37 we can obtain the daily averaged values of the cloud free $A_S(a_{mj}, t_{mj})$ and total cloud cover $A_c(a_{mj}, t_{mj}, \tau_c)$ albedos by using Eq. 40 as follows:

$$\bar{\mu}_{mj} = \frac{1}{2T_{mj}} \int_{-T_{mj}}^{T_{mj}} \mu_0(t)\,dt, \tag{55}$$

$$A_S(a_{mj}, t_{mj}) = \frac{1}{2T_{mj}} \int_{-T_{mj}}^{T_{mj}} A_S[a_{mj}, \theta_0(t)]\,[\mu_0(t)/\bar{\mu}_{mj}]\,dt, \tag{56}$$

$$A_c(a_{mj}, t_{mj}, \tau_c) = \frac{1}{2T_{mj}} \int_{-T_{mj}}^{T_{mj}} A_c[a_{mj}, \theta_0(t), \tau_c]\,[\mu_0(t)/\bar{\mu}_{mj}]\,dt, \tag{57}$$

where $t_{mj}$ indicates the value of a function averaged over the $j^{th}$ day of the $m^{th}$ month, and $t_m$ the value of the function averaged over the $j = 1, \ldots, N_m$ days of the $m^{th}$ month which has $N_m$ days. Equation 43 can now be used to relate these daily averaged albedos with daily averaged irradiances resulting in

$$W_S(a_{mj}, t_{mj}) = \bar{\mu}_{mj} H_{0S}(t_{mj}) A_S(a_{mj}, t_{mj}), \tag{58}$$

$$W_c(a_{mj}, t_{mj}, \tau_c) = \bar{\mu}_{mj} H_{0S}(t_{mj}) A_c(a_{mj}, t_{mj}, \tau_c), \tag{59}$$

$$W_{0S}(t_{mj}) = \bar{\mu}_{mj} H_{0S}(t_{mj}) \tag{60}$$

where $W_{0S}(t_{mj})$ is the daily averaged incident solar irradiance of Eq. 36, and the daily variation of $H_{0S}$ is noted due to the elliptical orbit of the earth about the sun causing the radius distance to vary.

In general the monthly averaged reflected and incident solar irradiances are given by

$$W_R(t_m) = \frac{1}{N_m} \sum_{j=1}^{N_m} W_R(t_{mj}), \tag{61}$$

$$W_{0S}(t_m) = \frac{1}{N_m} \sum_{j=1}^{N_m} \bar{\mu}_{mj} H_{0S}(t_{mj}) = \langle \bar{\mu}_{mj} H_{0S}(t_{mj}) \rangle . \tag{62}$$

The weighting function which satisfies our definition for the monthly averaged albedo

$$A(t_m) = \frac{W_R(t_m)}{W_{0S}(t_m)} = \frac{1}{N_m} \sum_{j=1}^{N_m} \left[ \frac{\bar{\mu}_{mj} H_{0S}(t_{mj})}{\langle \bar{\mu}_{mj} H_{0S}(t_{mj}) \rangle} \right] A(t_{mj}) \tag{63}$$

is therefore given by

$$w_{mj} = \bar{\mu}_{mj} H_{0S}(t_{mj}) / \langle \bar{\mu}_{mj} H_{0S}(t_{mj}) \rangle . \tag{64}$$

If we apply Eqs. 61 to 64 to the cloud free and total cloud cover cases we obtain the following monthly averaged irradiances and albedos:

$$W_S(t_m) = \langle \bar{\mu}_{mj} H_{0S}(t_{mj}) \rangle \, A_S(t_m) \tag{65}$$

$$W_c(t_m) = \langle \bar{\mu}_{mj} H_{0S}(t_{mj}) \rangle \, A_c(t_m) \tag{66}$$

$$A_s(t_m) = \frac{1}{N_m} \sum_{j=1}^{N_m} w_{mj} A_s(a_{mj}, t_{mj}), \tag{67}$$

$$A_c(t_m) = \frac{1}{N_m} \sum_{j=1}^{N_m} w_{mj} A_c(a_{mj}, t_{mj}, \tau_c). \tag{68}$$

We now address the problem of temporal averaging when fractional cloud cover occurs throughout the day. The daily averaged irradiance is obtained by combining Eqs. 21, 30, and 48 resulting in

$$W(a_{mj}, t_{mj}) = \frac{1}{2T_{mj}} \int_{-T_{mj}}^{T_{mj}} \left\{ [1 - f_c(t)] W_s(a_{mj}, \theta_0) + f_c(t) W_c[a_{mj}, \theta_0, \tau_c(t)] \right\} dt \tag{69}$$

where in general $f_c(t)$ and $\tau_c(t)$ have some diurnal dependence on t. If we use values of $f_c$ and $\tau_c$ which are constant over the day, but have mean values over the month, $f_c(t_m)$ and $\tau_c(t_m)$, which may vary from month to month then

$$\begin{aligned} W(a_{mj}, t_{mj}) &= [1 - f_c(t_m)] W_s(a_{mj}, t_{mj}) + f_c(t_m) W_c[a_{mj}, t_{mj}, \tau_c(t_m)] \\ &= \bar{\mu}_{mj} H_{0s}(t_{mj}) \left\{ [1 - f_c(t_m)] A_s(a_{mj}, t_{mj}) + f_c(t_m) A_c[a_{mj}, t_{mj}, \tau_c(t_m)] \right\} \end{aligned} \tag{70}$$

and the monthly averaged irradiance is

$$\begin{aligned} W(t_m) &= [1 - f_c(t_m)] W_s(t_m) + f_c(t_m) W_c(t_m) \\ &= \langle \bar{\mu}_{mj} H_{0s}(t_{mj}) \rangle \left\{ [1 - f_c(t_m)] A_s(t_m) + f_c(t_m) A_c[t_m, \tau_c(t_m)] \right\}, \end{aligned} \tag{71}$$

where the daily and monthly averaged albedos are

$$A[a_{mj}, t_{mj}, \tau_c(t_m), f_c(t_m)] = [1 - f_c(t_m)] A_S(a_{mj}, t_{mj}) + f_c(t_m) A_c[a_{mj}, t_{mj}, \tau_c(t_m)] \quad (72)$$

$$A(t_m) = [1 - f_c(t_m)] A_S(t_m) + f_c(t_m) A_c[t_m, \tau_c(t_m)] \, . \quad (73)$$

In CWN (1978) we use surface albedo climatology data, our parameterizations of $A_S(a, \theta_0)$ and $A_c(a, \theta_0, \tau_c)$, and the albedo model of Eq. 21 for total albedo, $A(a, \theta_0, \tau_c, f_c)$, for an atmosphere with fractional cloud cover, $f_c$, to compute monthly and zonally averaged values of $f_c$. Our values of A are obtained from the Nimbus 6 Earth Radiation Budget (ERB) instrument which is discussed by Smith et al., (1977). Consequently, our values of $f_c$ are only representative of the Nimbus 6 sampling times. If the diurnal behavior of cloud cover was known then it could be fit to our values of $f_c$ at these times to give $f_c(t)$, and Eq. 69 could be used to compute the daily averaged irradiance. Since this diurnal behavior is not known, in a subsequent paper we will use the values of $f_c(t_m)$ determined in CWN (1978) in Eqs. 70 to 73 to determine daily and monthly averaged values of irradiance and albedo.

Since Eq. 27 was used to determine $f_c$ at the ERB sampling time we know that the value of albedo and irradiance are consistent with the ERB values at that time of day. Our use of our parameterizations of $A_S(a, \theta_0)$ and $A_c(a, \theta_0, \tau_c)$ at other times of the day in Eqs. 56, 57, and 70 through 73 allows us to approximately solve the temporal sampling limitations of Nimbus 6 and compute proper time averages of albedo and irradiance.

Due to the simplicity of our $\theta_0$ parameterizations of $A_S(a, \theta_0)$ and $A_c(a, \theta_0, \tau_c)$ we will only need to compute $\bar{\mu}_{mj}$ and the weighted mean values of $\theta_0^n(t)$ defined by

$$\theta_{mj}^n = \frac{1}{2T_{mj}} \int_{-T_{mj}}^{T_{mj}} \theta_0^n(t) \, [\mu_0(t)/\bar{\mu}_{mj}] \, dt \tag{74}$$

for $n = 1, 2, 4,$ and 6 in order to obtain the daily averaged values of Eqs. 56 and 57. If we view the time dependent albedos to be specifically dependent on $\theta_0^n(t)$ as a polynomial instead of generally dependent on $\theta_0(t)$ then the daily averaged values of $A_S[a_{mj}, \theta_0^n(t)]$ and $A_c[a_{mj}, \theta_0^n(t), \tau_c]$ are obtained by substituting $\theta_{mj}^n$ for $\theta_0^n(t)$ in these functions, or

$$A_S(a_{mj}, t_{mj}) = A_S(a_{mj}, \theta_{mj}^n), \tag{75}$$

$$A_c(a_{mj}, t_{mj}) = A_c(a_{mj}, \theta_{mj}^n, \tau_c). \tag{76}$$

## 7. CONCLUSIONS

We have developed a simple parameterization of the extensive radiative transfer calculations of Dave and Braslau (1974, 1975) which should prove useful to many scientists in the areas of earth radiation budget, climate modeling, and climatological data analysis, and we ourselves will use these results in our future work. We have noted that the single cloud model of DB needs generalization and have attempted a reasonable approach to this problem.

The temporal and spatial sampling problem of satellite experiments designed to measure time averaged albedos and irradiances at the top of the atmosphere is discussed. We present how the use of our solar zenith angle parameterizations can allow proper time averages to be performed given satellite albedo measurements sampled at a few discrete times. By applying the definition of albedo consistently we derive the weighting functions needed to perform proper spectral and temporal averages of albedo.

## ACKNOWLEDGMENT

The research of one of the authors (MN) was supported by NASA under Contract NAS 5-24350. The reversal in the $A_c > A_s$ inequality was anticipated by Choudhury of Computer Sciences Corporation from his work on the reflectivity of snow and ice. He also notes that the albedo of snow or ice surfaces has a strong wavelength dependence which can cause the spectrally averaged albedo of snow or ice surfaces to differ when the atmospheric conditions above the surface are clear or cloudy.

## REFERENCES

Budyko, M., 1974: "Climate and Life." Academic Press, N. Y., pp. 112-113.

Curran, R. J., R. Wexler, and M. L. Nack, 1978: Albedo climatology analysis and the determination of fractional cloud cover. Submitted to the J. Appl. Meteor. for publication.

Dave, J. V., and N. Braslau, 1974: Effect of cloudiness on the transfer of solar energy through realistic model atmospheres. Rept. RC 4869, IBM T. J. Watson Research Center, Yorktown Heights, N. Y.

__________, and ________, 1975: Effect of cloudiness on the transfer of solar energy through realistic model atmospheres. J. Appl. Meteor., 14, 383-395.

Davis, J. M., S. K. Cox, and T. B. McKee, 1978: Solar absorption in clouds of finite horizontal extent. Proceedings of the Third Conference on Atmospheric Radiation, Davis, California, June 28-30, 195-197.

Jacobowitz, H., 1978. Private Communication.

Nack, M. L., and A. E. S. Green, 1974: Influence of clouds, haze, and smog on the middle ultraviolet reaching the ground. Appl. Optics, 13, 2405-2415.

Smart, W. M., 1965: Spherical Astronomy. Cambridge University Press, London, England.

Smith, W. L., J. Hickey, H. B. Howell, H. Jacobowitz, D. T. Hilleary, and A. J. Drummond, 1977: Nimbus-6 earth radiation budget experiment. Appl. Optics, 16, 306-318.

Vinnikov, K. Ia., 1965: Albedo of the system earth-atmosphere and the field of outgoing short-wave radiation. Tr. Gl. Geofiy. Observ. 170, 207-211.

Woerner, C. V., 1978: The earth radiation budget satellite system: an overview. Proceedings of the Third Conference on Atmospheric Radiation, Davis, California, June 28-30, 345-348.